Eur. Phys. J. D **6**, 523–532 (1999)

THE EUROPEAN PHYSICAL JOURNAL D

EDP Sciences
© Società Italiana di Fisica
Springer-Verlag 1999

Signal amplification by means of cavity solitons in semiconductor microcavities

L. Spinelli[1,a] and M. Brambilla[2]

[1] INFM, Dipartimento di Fisica, Università degli Studi di Milano, via Celoria 16, 20133 Milano, Italy
[2] INFM, Dipartimento Interateneo di Fisica, Politecnico di Bari, via E. Orabona 4, 7016 Bari, Italy

Received: 11 December 1998 / Received in final form: 25 February 1999

Abstract. Cavity solitons were recently predicted in semiconductor microresonators grown with a vertical geometry. By exploiting a previously introduced model valid for both passive and active configurations of a multiple-quantum-well device, we studied the response in the time domain offered by such self-organized structures in the device, when a small modulated optical signal is applied. Using appropriate symmetry considerations, the (2+1)-dimensional problem is reduced to a tractable form, by means of a semianalytical method. We demonstrated that large differential-gain factors, competitive with those of other all-optical and some opto-electronic devices, are attainable, when the output signal is collected at the peak of the cavity soliton. This fact, in connection with the reconfigurability properties already established for cavity soliton arrays, allows to conceive different schemes for optical information handling: feasible arrangements for parallel amplification and for signal commutation are proposed.

PACS. 42.65.Tg Optical solitons; nonlinear guided waves – 42.79.-e Optical elements, devices, and systems – 42.70.Nq Other nonlinear optical materials; photorefractive and semiconductor materials

1 Introduction

The possibility of using nonlinear optical systems to amplify an optical beam has motivated extended researches since the discovery of Optical Bistability (see, *e.g.*, [1]). The intensity of a coherent beam, injected into the device, yields an output beam of higher intensity. The amplification ratio is generally referred to as "dc gain", adopting a terminology derived from electronics. Another interesting application lies in the amplification of oscillations in the injected beam intensity, in which case the information is thought to reside in the carrier beam modulation. In this case the "differential gain" is introduced, as a measure of the oscillation amplification ratio between the input and the output beam.

In recent years, schemes for all-optical transistor operation in nonlinear optical systems have been proposed for several devices, including nonlinear crystals capable of parametric conversion, semiconductor devices, lasers with injected signal, photorefractive media and liquid crystal light valves. Semiconductor devices and χ^2 media offer the bonus of fast time response and device compactness; the former, in addition, lend themselves to applications where optical signals are interfaced with microelectronic circuit units for electro-optical signal amplification or processing [2].

One limitation, so far, has been the physical dimensions of the nonlinear optical component: each single beam, thought as the signal carrier, has to be processed by one nonlinear element and gives rise to one output beam (output signal). If several signals must be treated in parallel, then one must, *e.g.*, ensure suitable means to isolate the active (amplifying) elements to avoid pixel crosstalk. In addition, tight focusing of the beams on the material is discouraged because of diffractive divergence. In semiconductor devices a widely adopted technique is the etching of arrays of monolithic elements in a wafer, a typical case being that of Vertical-Cavity Surface-Emitting Lasers (VCSELs). There, physical separation of the material structures guarantees radiation as well as carrier plasma confinement and thus pixel independence. Of course, micromachining material structures makes the pixel location fixed, requiring accurate beam addressing and readout, along with a loss of flexibility as for array reconfigurability and fanning.

In the recent few years theoretical researches and fewer experimental demonstrations have shown the possibility of realizing self-organized isolated intensity peaks in the transverse profile of a coherent field interacting with a nonlinear planar resonator (see, *e.g.*, [3,4]). These peaks have a solitonic character in the sense that they do not experience diffractive broadening and several such structures can be independently switched on and off in a broad area device [5]. They are commonly designated as Cavity Solitons (CS).

A major breakthrough has been represented by the prediction of such structures in a semiconductor

[a] e-mail: lorenzo.spinelli@mi.infn.it

microresonator based on a GaAs/AlGaAs Multiple Quantum Well (MQW) active medium [6]. Theoretical models and simulations predict that a 3×3 matrix of such self-organized pixels could be realized in a resonator having a 100×100 μm cross-section. Although this figure is far from challenging microelectronic circuitry, it could be interesting when compared to single smart pixels which, adding altogether the optical resonator and the electronic interface, scale up to 0.3–1 mm^2 [7]. As will be illustrated in the following sections, CS can be operated as optical transistors for amplifying signal modulation. A differential gain factor has been found, which is quite sizable when compared to similar figures for other all-optical devices, and to some electro-optical ones, to the best of our knowledge [8–11].

The characterization of CS in semiconductor devices has been extensively carried out in [12] and the reader is referred to that work for an overview of their characteristics. Here we will concentrate on the oscillation amplification regime when the injected beam is temporally modulated.

For the scope of this work, let it suffice to remind that CS are single intensity peaks appearing in the transverse field profile emitted by a broad area semiconductor microresonator. They are stationary structures which are sustained by an injected plane-wave field, and can be switched on and off by suitably addressed pulses superimposed to the injected field profile. CS created at distances larger than a certain critical distance (roughly equal to the same CS size) remain independent of one another. Thus CS can be thought as light pixels "written" in the transverse section of the device with no need of pixel etching in the medium.

Once the concept of light pixel has been brought in, it appears natural to evaluate its response in the time domain to oscillations. In Section 2 we evaluate the linear response of the CS, introducing a new approach with respect to what has been done in the past [13,14] where the variable whose response was sought never exhibited space dependence. In Section 3 we estimate the figures of merit which we consider relevant for optical transistor operation. Section 4 contains the numerical results and their comparison to theoretical predictions, and Section 5 offers some discussions about what has been obtained and the perspectives of applications for CS-based all-optical devices.

2 The model and the linearized equations

We consider a broad area semiconductor heterostructure both in the passive and in the active configuration. The semiconductor microresonator is of the Fabry-Pérot type, with a MQW structure perpendicular to the direction z of propagation of the radiation.

The mathematical model appropriate to describe this device was stated in two recent works [6,12]. We apply the mean field limit because the high-Q cavity is quite short, and eliminate the longitudinal coordinate z, thus assuming that only one longitudinal cavity mode is relevant to the dynamics of the system; we then obtain a set of partial differential equations for the temporal evolution of the electric field inside the cavity and of the carrier density describing the semiconductor material:

$$\frac{\partial E}{\partial t} = -(1+\eta+i\theta)E + E_I - 2Ci\Theta(N-1)E + i\nabla_\perp^2 E\,, \quad (1a)$$

$$\frac{\partial N}{\partial t} = -\gamma\left[N+\beta N^2 - J + |E|^2(N-1) - d\nabla_\perp^2 N\right]\,, \quad (1b)$$

where E is the normalized slowly varying envelope of the electric field and N is the carrier density, normalized to its transparency value. The Laplacian operator

$$\nabla_\perp^2 = \frac{\partial^2}{\partial x^2} + \frac{\partial^2}{\partial y^2}\,, \quad (2)$$

describes diffraction in the paraxial approximation, with the transverse coordinates x, y scaled to the square root of the diffraction length. On the other hand, time is scaled to the photon lifetime in the cavity. The parameter η accounts for the linear absorption due to the material in the regions between the quantum wells and the mirrors; θ is the cavity detuning parameter; C is the bistability parameter; γ is the nonradiative recombination rate of the carriers; β is the coefficient of the radiative recombination involving two carriers; d is the diffusion coefficient of the carriers; J is the intensity of the pump current, normalized to its transparency value. E_I is the slowly varying envelope the coherent electric field driving the microresonator. Equations (1a, 1b) can be used to describe the microresonator both in passive and in active configuration (VCSEL). The modellistic difference between the two configurations of the device lies in the parameter Θ: in particular, for the passive configuration $\Theta = \frac{\Delta+i}{1+\Delta^2}$, where Δ is the detuning parameter with respect to the central frequency of the excitonic absorption line, approximated by Lorentzian shape [15], while for the active configuration $\Theta = \alpha + i$ [16], where α is the linewidth enhancement factor [17]. The pump current J is nonvanishing only in the active case, where the medium is inverted, but the laser is kept some 5-10% below threshold to avoid spatio-temporal and polarization instabilities typical of semiconductor emitters.

It is known [6,12] that for suitable choices of the parameters the system can undergo a modulational instability [18] which causes a pattern-forming process. As an outcome there exist stationary solutions where the electric field transverse profile $E(x,y)$ is not homogeneous, even if the injected field E_I is homogeneous. An example of plane-wave stationary solution with the characteristic S-shape typical of bistability is plotted as a full line in Figure 1; here the branches of the patterned stationary solutions are also shown. Among these spatially modulated solutions there exists a stationary solution in the form of a peak of light, its intensity corresponding to the value of the black dot in the figure, embedded in a darker homogeneous background, corresponding to the coexisting plane-wave solution of the lower branch in the figure.

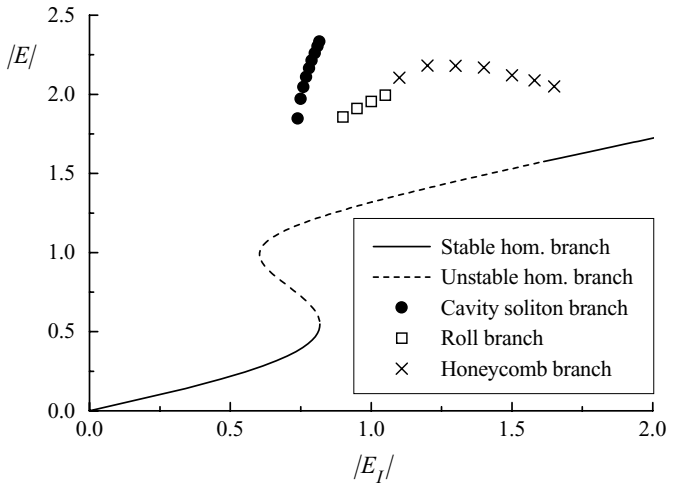

Fig. 1. Example of a homogeneous steady-state curve and branches of patterned stationary solutions in the active case. Parameters are: $C = 0.45$, $\theta = -2$, $\alpha = 5$, $I = 2$, $d = 0.052$, $\eta = 0$, $\beta = 0$.

Of course, this is the CS introduced above (see Fig. 6b). All stable CS we met exhibit cylindrical symmetry around the peak.

If we wish to make the CS peak oscillate, the most intuitive idea is to modulate in time the homogeneous injected field. By looking at the soliton branch in Figure 1, one immediately realizes that it is much steeper than the plane-wave high-transmissivity branch. For slow enough modulations the response of the CS is expected to scale with the first derivative of the soliton branch. So a sizable enhancement of the oscillations can be foreseen. The approach must obviously be more rigorous: the precise differential gain factor for small signals can only be evaluated by calculating the linear response curve of the system at the CS peak.

To this aim, we assume the driving field E_I constituted by a homogeneous background contribution $E_\mathrm{I}^{(\mathrm{hom})}$ and a small signal e_I modulated in time:

$$E_\mathrm{I} = E_\mathrm{I}^{(\mathrm{hom})} + e_\mathrm{I}(r;t)\,, \tag{3}$$

where $r = \sqrt{x^2+y^2}$ is the radial space variable in the transverse plane. We allowed for the small injected signal also the possibility of a spatial structure with the same cylindrical symmetry as the cavity soliton.

If e_I is small enough, the variables of the system will react linearly. Then, we can assume for E and N the following form:

$$E(r;t) = E_\mathrm{S}(r) + e(r;t)\,, \tag{4a}$$
$$N(r;t) = N_\mathrm{S}(r) + n(r;t)\,, \tag{4b}$$

where $E_\mathrm{S}(r)$ and $N_\mathrm{S}(r)$ are the stationary solutions corresponding to a cavity soliton at $r = 0$. For symmetry reasons, we assume that the response of the system has a radial dependence on the transverse variables.

By substituting equations (3, 4a, 4b) into equations (1a, 1b) and linearizing with respect to the small quantities $e(r;t)$, $n(r;t)$, $e_\mathrm{I}(r;t)$, we obtain the following equations:

$$\frac{\partial e}{\partial t} = -(1+\eta+i\theta+2Ci\Theta(N_\mathrm{S}-1))e - 2Ci\Theta E_S n + i\nabla_\perp^2 e + e_\mathrm{I}\,, \tag{5a}$$
$$\frac{\partial n}{\partial t} = -\gamma\left\{(1+2\beta N_\mathrm{S}+|E_\mathrm{S}|^2)n + E_\mathrm{S}^*(N_\mathrm{S}-1)e + E_\mathrm{S}(N_\mathrm{S}-1)e^* - d\nabla_\perp^2 n\right\}. \tag{5b}$$

Moreover, we will assume for the small quantities $e_\mathrm{I}(r;t)$, $e(r;t)$, $n(r;t)$ the following dependence on time:

$$e_\mathrm{I}(r;t) = \tilde{e}_\mathrm{I}(r;\omega)\mathrm{e}^{-i\omega t} + \tilde{e}_\mathrm{I}(r;-\omega)\mathrm{e}^{i\omega t}\,, \tag{6a}$$
$$e(r;t) = \tilde{e}(r;\omega)\mathrm{e}^{-i\omega t} + \tilde{e}(r;-\omega)\mathrm{e}^{i\omega t}\,, \tag{6b}$$
$$n(r;t) = \tilde{n}(r;\omega)\mathrm{e}^{-i\omega t} + \tilde{n}(r;-\omega)\mathrm{e}^{i\omega t}\,. \tag{6c}$$

By substituting these expressions into the linear equations (5a, 5b) and comparing the terms with the same exponential part, we obtain the following equation for the variables $\tilde{e}$, $\tilde{e}_*$ and $\tilde{n}$, where $\tilde{e}_*(r;\omega) = \tilde{e}^*(r;-\omega)$:

$$-i\gamma\bar{\omega}\tilde{e} = A(r)\tilde{e} + B(r)\tilde{n} + i\nabla_\perp^2\tilde{e} + \tilde{e}_\mathrm{I}\,, \tag{7a}$$
$$-i\gamma\bar{\omega}\tilde{e}_* = A^*(r)\tilde{e}_* + B^*(r)\tilde{n} - i\nabla_\perp^2\tilde{e}_* + \tilde{e}_{\mathrm{I}*}\,, \tag{7b}$$
$$-i\bar{\omega}\tilde{n} = C(r)\tilde{n} + D(r)\tilde{e} + D^*(r)\tilde{e}_* + d\nabla_\perp^2\tilde{n}\,. \tag{7c}$$

Here we rescaled the frequency to γ, $\bar{\omega} = \omega/\gamma$, and we set

$$A(r) = -\left[1+\eta+i\theta+2Ci\Theta(N_\mathrm{S}(r)-1)\right], \tag{8a}$$
$$B(r) = -2Ci\Theta E_\mathrm{S}(r)\,, \tag{8b}$$
$$C(r) = -\left[1+2\beta N_\mathrm{S}(r)+|E_\mathrm{S}(r)|^2\right], \tag{8c}$$
$$D(r) = -E_\mathrm{S}^*(r)\left(N_\mathrm{S}(r)-1\right). \tag{8d}$$

Incidentally, from equation (7c) it derives that $\tilde{n}_*$ satisfies the same equation for $\tilde{n}$ and, hence, $\tilde{n}_* = \tilde{n}$, that is $n(r;t)$ is real, as it must be.

For the sake of simplicity, we will consider the case without diffusion of the carriers. In reference [12] we show that the system can be treated with similar techniques in the limiting cases when the diffusion is either large or small, provided suitable expansions are introduced. Then, in the following we will set $d = 0$. With this assumption, by means of equations (7c) we can express $\tilde{n}$ as a function of $\tilde{e}$ and $\tilde{e}_*$:

$$\tilde{n} = -\frac{D(r)}{i\bar{\omega}+C(r)}\tilde{e} - \frac{D^*(r)}{i\bar{\omega}+C(r)}\tilde{e}_*\,. \tag{9}$$

Once substituted this expression into equations (7a, 7b), we obtain the final couple of equations for the small quantities $\tilde{e}$, $\tilde{e}_*$:

$$\nabla_\perp^2\tilde{e} = -i\left[\chi\tilde{e} + \zeta\tilde{e}_* - \tilde{e}_\mathrm{I}\right], \tag{10a}$$
$$\nabla_\perp^2\tilde{e}_* = i\left[\zeta_*\tilde{e} + \chi_*\tilde{e}_* - \tilde{e}_{\mathrm{I}*}\right], \tag{10b}$$

where we introduced the coefficients:

$$\chi(r;\omega) = -i\gamma\bar{\omega} - A(r) + \frac{D(r)B(r)}{i\bar{\omega}+C(r)}\,, \tag{11a}$$
$$\zeta(r;\omega) = \frac{D^*(r)B(r)}{i\bar{\omega}+C(r)}\,. \tag{11b}$$

Equations (10a, 10b) can be solved numerically by exploiting the *shooting method* described in [6]. In essence this method relies on a radial integration of the equations (10a, 10b) starting from initial conditions at $r = 0$ which are adaptively "shot at", by matching the homogeneous solution to which the CS must connect at $r \longrightarrow \infty$. The initial condition is determined by imposing that the solution for $r \to +\infty$ becomes constant: the values which the solution approaches can be obtained by equations (10a, 10b), dropping the Laplacian terms:

$$\tilde{e}^{(\mathrm{hom})} = \frac{\chi_*^{(\mathrm{hom})}\tilde{e}_{\mathrm{I}} - \zeta^{(\mathrm{hom})}\tilde{e}_{\mathrm{I}*}}{\chi^{(\mathrm{hom})}\chi_*^{(\mathrm{hom})} - \zeta^{(\mathrm{hom})}\zeta_*^{(\mathrm{hom})}}\,, \qquad (12a)$$

$$\tilde{e}_*^{(\mathrm{hom})} = \frac{\chi^{(\mathrm{hom})}\tilde{e}_{\mathrm{I}*} - \zeta_*^{(\mathrm{hom})}\tilde{e}_{\mathrm{I}}}{\chi^{(\mathrm{hom})}\chi_*^{(\mathrm{hom})} - \zeta^{(\mathrm{hom})}\zeta_*^{(\mathrm{hom})}}\,; \qquad (12b)$$

here $\chi^{(\mathrm{hom})}$ and $\zeta^{(\mathrm{hom})}$ are the expressions (11a, 11b) evaluated at the homogeneous values of E_{S} and N_{S}.

3 Maximum amplification coefficient

From equations (10a, 10b), we obtain, for each couple of functions $\tilde{e}_{\mathrm{I}}$, $\tilde{e}_{\mathrm{I}*}$, a couple of functions $\tilde{e}$, $\tilde{e}_*$. While the above relations are formulated for the intracavity field, the quantity which is really relevant for applications is the field emerging from the output mirror. Indeed, from the input-output relations of the microcavity, the output field is normalized in the same way as the input one and coincides with the intracavity field. The explicit calculations are reported in Appendix A. Then, we can consider straightforwardly $\tilde{e}$, $\tilde{e}_*$ as the output signal field, in order to obtain the amplification coefficient of the injected signal $\tilde{e}_{\mathrm{I}}$, $\tilde{e}_{\mathrm{I}*}$.

More precisely, one can observe that, once defined the radial profile of the functions $\tilde{e}_{\mathrm{I}}$, $\tilde{e}_{\mathrm{I}*}$, the correspondence between the complex vectors $\mathbf{e}_{\mathrm{I}} = (\tilde{e}_{\mathrm{I}}(r=0), \tilde{e}_{\mathrm{I}*}(r=0))$ and $\mathbf{e} = (\tilde{e}(r=0), \tilde{e}_*(r=0))$ (output signal collected at the peak of the cavity soliton) is linear, that is a 2×2 complex matrix. The maximum amplification of the input signal occurs when the input signal vector $(\tilde{e}_{\mathrm{I}}(r=0), \tilde{e}_{\mathrm{I}*}(r=0))$ is an eigenvector of that matrix, corresponding to the suitable eigenvalue [13]. If we assume that $\mathbf{e}_{\mathrm{I}}$ is the eigenvector relative to the eigenvalue λ, that is

$$\mathbf{e} = \lambda \mathbf{e}_{\mathrm{I}}\,, \qquad (13)$$

the output signal (6b) can be written in the following way:

$$e = |\lambda| \left\{ |\tilde{e}_{\mathrm{I}}| \mathrm{e}^{-i\omega t + i\psi} + |\tilde{e}_{\mathrm{I}*}| \mathrm{e}^{i\omega t - i\psi} \right\} \mathrm{e}^{i\delta}\,, \qquad (14)$$

where

$$\psi = \frac{\varphi_{\mathrm{I}} + \varphi_{\mathrm{I}*}}{2} + \varphi_\lambda\,, \qquad \delta = \frac{\varphi_{\mathrm{I}} - \varphi_{\mathrm{I}*}}{2}\,, \qquad (15)$$

and

$$\tilde{e}_{\mathrm{I}} = |\tilde{e}_{\mathrm{I}}| \mathrm{e}^{i\varphi_{\mathrm{I}}}\,, \quad \tilde{e}_{\mathrm{I}*} = |\tilde{e}_{\mathrm{I}*}| \mathrm{e}^{i\varphi_{\mathrm{I}*}}\,, \quad \lambda = |\lambda| \mathrm{e}^{i\varphi_\lambda}\,. \qquad (16)$$

On the other hand, we can recast the input signal (6a) as

$$e_{\mathrm{I}} = \left\{ |\tilde{e}_{\mathrm{I}}| \mathrm{e}^{-i\omega t + i\psi_{\mathrm{I}}} + |\tilde{e}_{\mathrm{I}*}| \mathrm{e}^{i\omega t - i\psi_{\mathrm{I}}} \right\} \mathrm{e}^{i\delta}\,, \qquad (17)$$

where

$$\psi_{\mathrm{I}} = \frac{\varphi_{\mathrm{I}} + \varphi_{\mathrm{I}*}}{2}\,. \qquad (18)$$

Next, we consider the intensities of the input and output signals, because these are the quantities that can be experimentally measured:

$$|e_{\mathrm{I}}|^2 = \left(|\tilde{e}_{\mathrm{I}}| + |\tilde{e}_{\mathrm{I}*}|\right)^2 \cos^2(\omega t - \psi_{\mathrm{I}}) + \left(|\tilde{e}_{\mathrm{I}}| - |\tilde{e}_{\mathrm{I}*}|\right)^2 \sin^2(\omega t - \psi_{\mathrm{I}})\,, \qquad (19)$$

$$|e|^2 = |\lambda|^2 \left\{ \left(|\tilde{e}_{\mathrm{I}}| + |\tilde{e}_{\mathrm{I}*}|\right)^2 \cos^2(\omega t - \psi) + \left(|\tilde{e}_{\mathrm{I}}| - |\tilde{e}_{\mathrm{I}*}|\right)^2 \sin^2(\omega t - \psi) \right\}\,. \qquad (20)$$

These expressions show that the intensities of the input and output signals are proportional, apart from the phase of the eigenvalue λ which is present in the phase factor ψ and not in ψ_{I} (compare expressions (15) and (18)). Then, we can define as amplification coefficient the quantity

$$\Gamma = |\lambda|^2\,. \qquad (21)$$

In this way the input signal vector $\mathbf{e}_{\mathrm{I}}$, which experiences the maximum amplification, is the eigenvector corresponding to the eigenvalue with the largest modulus.

The amplification coefficient Γ can be calculated numerically, exploiting the shooting method [6] to integrate the equations (10a, 10b) and, then, to evaluate the eigenvalue λ with the largest modulus. On the other hand, if we consider the plane-wave case in which we use as stationary solution E_{S}, N_{S} the homogeneous values relative to the lower branch of the steady-state curve, the Laplacian terms in equations (10a, 10b) can be dropped and the amplification coefficient can be calculated analytically [13, 14]. As expected amplification factors are smaller in this latter case due to the smaller slope of the lower branch of the steady-state curve with respect to the slope of the CS branch. It results that both in the passive and in the active configurations the amplification factor Γ for plane-wave modulation is hardly larger than 1. On the contrary, we will see in the next section that things considerably improve when CS are involved.

4 Discussion of results

We first report some numerical results about the amplification coefficient Γ, obtained by integrating the linearized equations (5a, 5b) by means of the *shooting method*, and compare them to analogous results obtained under the same conditions (amplitude of the modulated signal equal to 1% of the background driving field: this is enough to preserve linear regime) performing a direct integration of

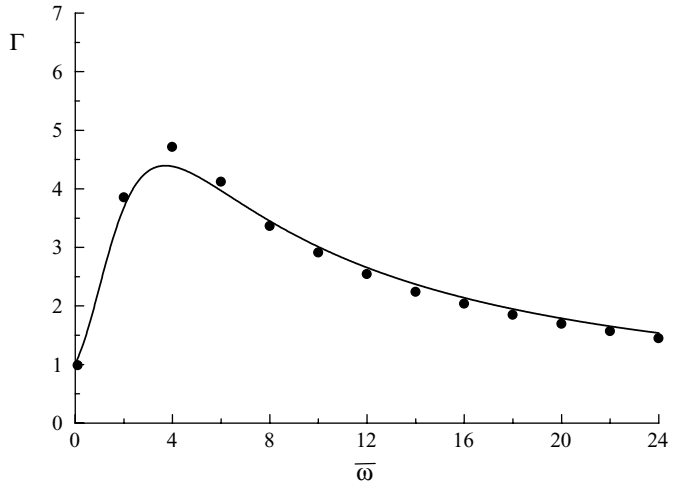

Fig. 2. Amplification coefficient Γ as a function of the modulation frequency $\bar{\omega}$ in the case of the passive configuration. Solid line: *shooting method*; •: split-step method. Parameters: $C = 40$, $\theta = -2$, $\Delta = 1$, $J = 0$, $\gamma = 0.002$, $\beta = 1.6$, $\eta = 0.25$, $d = 0$, $E_{\mathrm{I}}^{(\mathrm{hom})} = 31$.

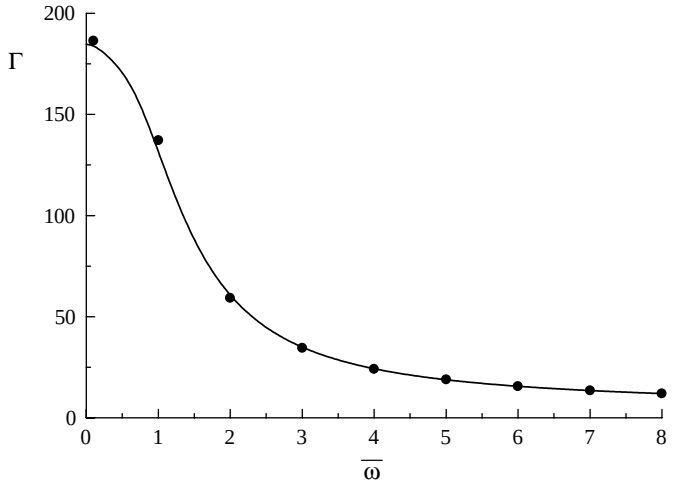

Fig. 3. Amplification coefficient Γ as a function of the modulation frequency $\bar{\omega}$ in the case of the active configuration. Solid line: *shooting method*; •: split-step method. Parameters: $C = 0.45$, $\theta = -2$, $\alpha = 5$, $J = 2$, $\gamma = 0.012$, $\beta = \eta = d = 0$, $E_{\mathrm{I}}^{(\mathrm{hom})} = 0.75$.

the equations (1a, 1b) by means of a split-step method with excellent agreement.

In Figures 2 and 3 two examples are reported, where the input signal is homogeneous in the transverse plane. From these figures one can note that high amplification coefficients can be obtained, especially in the active configuration (see Fig. 3). In this case we can also estimate the bandwidth for the modulation amplification, taking the resonance width at half height. By introducing realistic parameters for GaAs/AlGaAs heterostructures in a high reflectivity Bragg microresonator [12], we can expect a bandwidth of about 300 MHz.

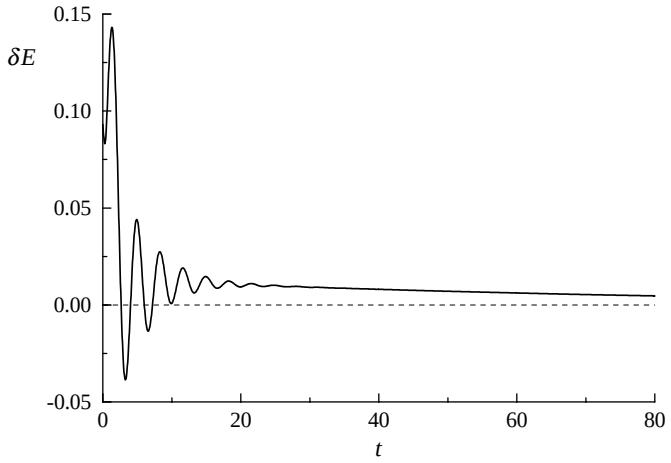

Fig. 4. Time evolution of an initial perturbation affecting the electric field E at CS peak, in the active configuration. The long nonoscillating decay is exponential with a damping time $\tau = 75.8$. Parameters are the same as in Figure 3.

One would expect that the frequency response of the system to the modulated input signal just evidenced is linked to the damping time of the perturbations affecting the CS at regime. In order to show that this is the case, we have performed some numerical simulations where we observed how a small perturbation δE introduced in the stable steady state with a CS relaxes during the time evolution of the system.

In Figure 4 we report the time evolution of a small perturbation affecting the CS peak, in the case of the active configuration. We note the presence of two time scales in the damping process of the CS perturbation: a faster, oscillating damping and a slower, nonoscillating damping. This behavior can be heuristically understood if we analyze the behavior of the plane-wave relaxation dynamics. To this purpose we performed a linear stability analysis of the homogeneous steady state of equations (1a, 1b) (see Appendix B). From Figure 4 one can derive a long decay rate $\tau^{-1} = 1.32 \times 10^{-2}$. The frequency response of the system is given by the Fourier transform of the damping function and it results a Lorentzian with a half-width $\omega_0 = \tau^{-1}$. The amplification coefficient Γ as a function of the input signal frequency $\bar{\omega}$ reported in Figure 3, can be well fitted by a Lorentzian function with a half-width $\bar{\omega}_0 = 1.2$. By comparing this value with $\bar{\omega}_0 = 1.1$ obtained by normalizing τ^{-1} to γ, we have a clear evidence of the direct link between the frequency response of the system and the damping of perturbations.

Also in the passive case two time scales can be evidenced in the exponential damping of a perturbation affecting the CS peak (see Fig. 5). The longer one would give a Lorentzian curve with a half-width $\bar{\omega}_0 = 4.85$ for the frequency response. Even if it is more difficult to extrapolate a Lorentzian shape from the plot reported in Figure 2, the half-width of the curve therein is about the same as $\bar{\omega}_0$ given above. Despite this link between relaxation timescales and CS resonance cutoff, it appears that a similar link does not exist for the resonance peak, which could be

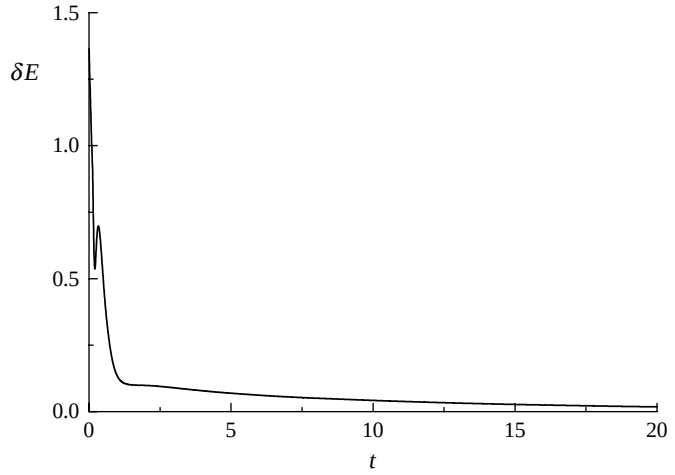

Fig. 5. Time evolution of an initial perturbation affecting the electric field E at CS peak, in the passive configuration. The long nonoscillating decay is exponential with a damping time $\tau = 103.1$. Parameters are the same as in Figure 2.

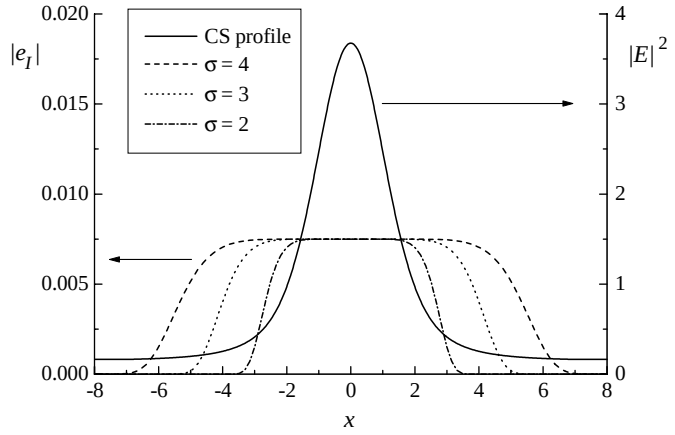

Fig. 6. Cross section of the input field with the super-Gaussian transverse profile (22) compared with the CS transverse cross section, in the case of the active configuration. Parameters are the same as in Figure 3.

intuitively expected to be related to the relaxation oscillations of the CS peak. The same simulations performed above did not offer an unambiguous interpretation for the position of the resonance peak (about $\bar{\omega} = 0$ for the active case, $\bar{\omega} = 4$ for the passive one).

It may be objected that modulating in time the whole homogeneous input beam requires a rather large input signal power, given that the device is broad-area. By adopting typical parameter values as above, holding powers for E_{I} can be on the order of 500 mW in the passive case and 50 in the active one [12]. This has motivated us to maintain the input homogeneous field constant and to superimpose thereon a narrow super-Gaussian pulse bearing the modulation in time, in such a way that the amplitude

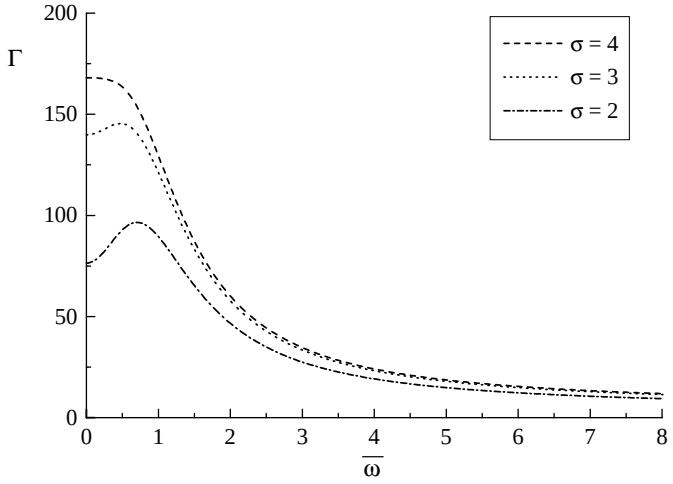

Fig. 7. Amplification coefficient Γ as a function of the modulation frequency $\bar{\omega}$, relative to the super-Gaussian input signals of Figure 6.

of the small input signal (6a) reads

$$\tilde{e}_{\mathrm{I}} = \tilde{e}_{\mathrm{I}}^{(\mathrm{hom})} \exp\left[-\left(\frac{r^2}{2\sigma^2}\right)^4\right]. \tag{22}$$

In Figure 6 we show the profile of the input signal compared with the profile of the stationary cavity soliton. In Figure 7 we report the relative amplification coefficients as a function of the modulation frequency in the case of the active configuration. We do not provide an analogous curve for the passive configuration because the gain factors attainable in this case are less interesting. We note that the amplification coefficient is decreased with respect to the case of homogeneous input signal, but it is still large as long as the region where the input signal is nonvanishing almost coincides with the region where the cavity soliton is nonvanishing. Since the power scales as the intensity by the pulse area, now the input signal power required for amplification is considerably lowered (by a factor 10 for $\sigma = 4$ in equation (22)).

We note, moreover, that the resonance peak shifts in the gain spectrum to higher frequencies $\bar{\omega} > 0$, like in the passive configuration (compare Fig. 2), when the input signal has a radial dependence while the bandwidth is not dramatically affected. By adopting perturbative approaches, we could not provide a quantitative motivation for this shift.

Another set of simulations was devoted to estimate the frequency response of the system to the monochromatic input signal. In the linear limit, by definition, the output signal is characterized by the same frequency as the input one. If we relax this approximation, however, due to the nonlinearity of the system, we expect that in the output modulation also the harmonics of the injected frequency are present. This is, in fact, what happens when the amplitude of the input field is large enough (with respect to the background) to go beyond the linear limit; in Figures 8 and 9 we show the power spectra of the output

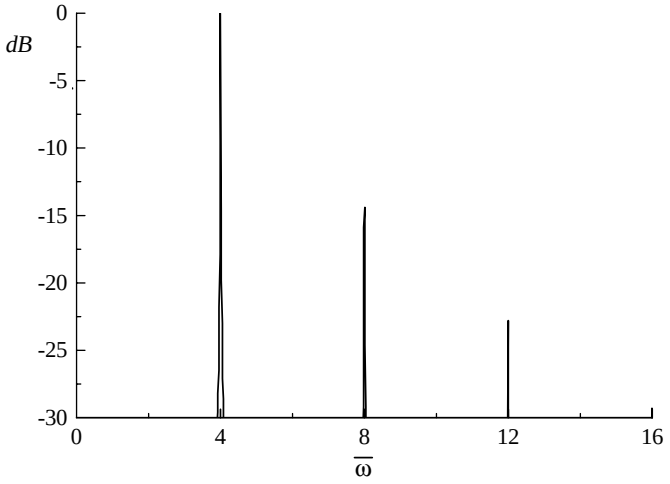

Fig. 8. Power spectrum of the output signal, in the case of the passive configuration. The spectrum is scaled to the value at the modulation frequency $\bar{\omega} = 4$. The amplitude of the input signal is 5% of $E_{\mathrm{I}}^{(\mathrm{hom})}$. Parameters: $C = 40$, $\theta = -2$, $\Delta = 1$, $J = 0$, $\gamma = 0.002$, $\beta = 1.6$, $\eta = 0.25$, $d = 0$, $E_{\mathrm{I}}^{(\mathrm{hom})} = 31$.

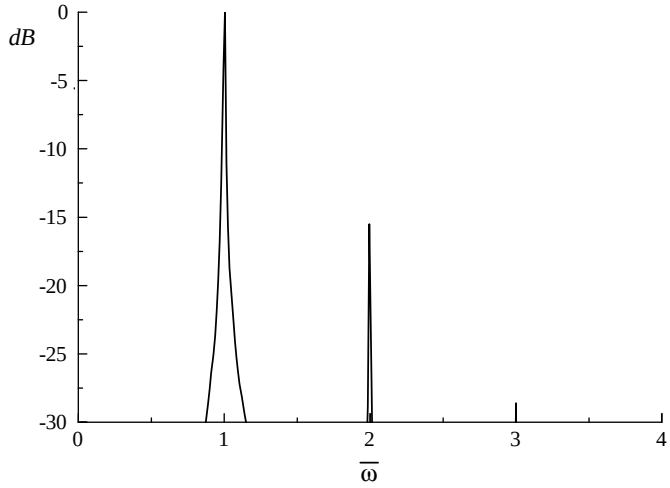

Fig. 9. Power spectrum of the output signal, in the case of the active configuration. The spectrum is scaled to the value at the modulation frequency $\bar{\omega} = 1$. The amplitude of the input signal is 15% of $E_{\mathrm{I}}^{(\mathrm{hom})}$. Parameters: $C = 0.45$, $\theta = -2$, $\alpha = 5$, $J = 2$, $\gamma = 0.012$, $\beta = \eta = d = 0$, $E_{\mathrm{I}}^{(\mathrm{hom})} = 0.78$.

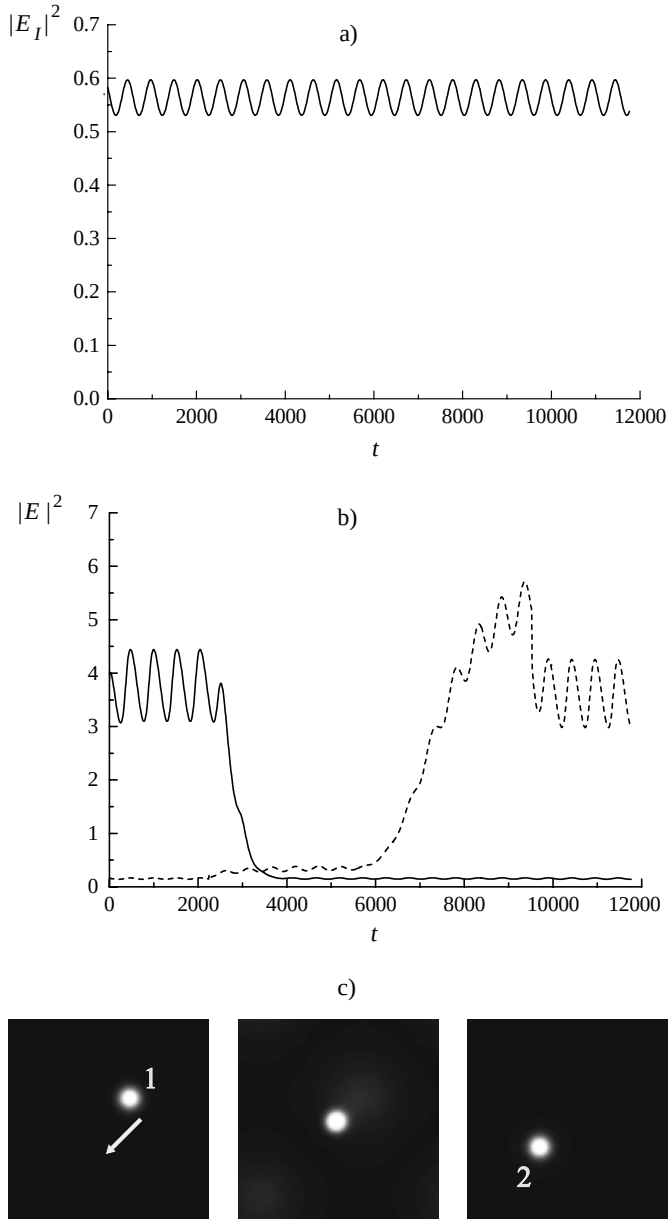

Fig. 10. Example of the commutation scheme for the input signal of frequency $\bar{\omega} = 1$ (a): output signal (b) collected at detector 1 (solid line) and at detector 2 (dashed line). The commutation is provided by the shifting cavity soliton (c) from position 1 to position 2 of the transverse plane. Parameters are the same as in Figure 3.

signals for both the passive and the active configurations: the presence of higher harmonics of the main frequency is evident; in this way an array of CS can be regarded as a parallel device where each pixel acts as a multiplier channel for the particular frequency, which modulates the super-Gaussian pulse applied at the CS location. Turning the CS on and off activates and inhibits the amplifying channels for selected frequency components with no need to act on the input signal. Furthermore, we observed that the linewidth at the fundamental frequency in output is the same we have in the input (we do not show here the input spectra for sake of shortness): this fact may suggest that the signal-to-noise ratio in input could not be heavily degraded in the amplification process. A quantitative evaluation of the signal-to-noise ratio enhancement factors is under preliminary investigation.

We also studied the dependence of the amplification coefficient as a function of the input signal amplitude in the nonlinear limit: we found that Γ is only weakly dependent on the signal amplitude, varying of about 10% when the signal modulation is brought from 1% to 5% of the background (we do not show here any plot about this).

The amplifying properties of CS just demonstrated, in connection with their dynamical properties, allow to

conceive different ways to process the input signal. As an example, one can commute the input signal from one position of the transverse plane to another one. In Figure 10 we report the output signals collected at two different positions of the transverse plane. The cavity soliton is modulated by the homogeneous field (Fig. 10a). A phase gradient is superimposed to this time-dependent background and the soliton consequently shifts from position 1 to position 2 (Fig. 10c). The signal collected by two detectors at locations 1 and 2 shows the signal commutation between the two channels (Fig. 10b). In this way the carrier signal (the oscillation of the plane wave) coexists in the same "channel" (the input field) with the switching signal (the phase gradient), and the result is the output signal (the modulated intensity collected by the detector) switching from one output channel (the detector at position 1) to the other (the detector at position 2).

In the previous analysis, we defined the maximum amplification coefficient as the ratio of the intensity of the input signal to that of the output signal collected at the CS peak. What is actually observed when the radiation is collected by a detector is the modulation of the output power, integrated over the detector area. For narrow detection areas, this is the power associated to the whole CS (its intensity integrated over soliton size). However, we verified that the size of the CS is practically constant during the oscillations, so that the power is simply proportional to the intensity at $r = 0$; then Γ can be referred to as the gain factor.

5 Conclusions

In this work we have evidenced that CS can efficiently amplify oscillations of an input optical beam. The differential gain factor in both passive and active configurations can confront those of other devices described in literature for similar applications. Moreover, the connection between amplifying properties and the damping time of perturbations exhibited by CS was stressed.

In the main body of the paper we discussed the most interesting features related to operations limited to a single soliton. Indeed the appealing side of CS is their possibility of being organized in reconfigurable arrays, and it has been shown [12,19,20] that they can be shifted to any desired location in the transverse field profile by applying proper phase or intensity gradients to the input field. While the investigations are still in an initial phase, we are studying the mechanisms by which input fields can steer two or more modulated CS.

As an example, we verified that, if there are two CS simultaneously present in the transverse plane at such a relative distance that they are independent of one another, each of them can amplify an input signal of different frequency, provided that each one is injected by using a super-Gaussian pulse as described above. There is no evidence of reciprocal interference. This feature is interesting for the parallel amplification of two or more signals and, in connection with the showed nonlinear response of the input/output characteristics, also for parallel frequency multiplication.

Furthermore, with the aim of performing all-optical signal processing by means of CS-based devices, we proposed a reliable scheme for the realization of signal commutation among different transmitting channels in the transverse plane: it relies on the dynamical and amplifying properties exhibited by CS.

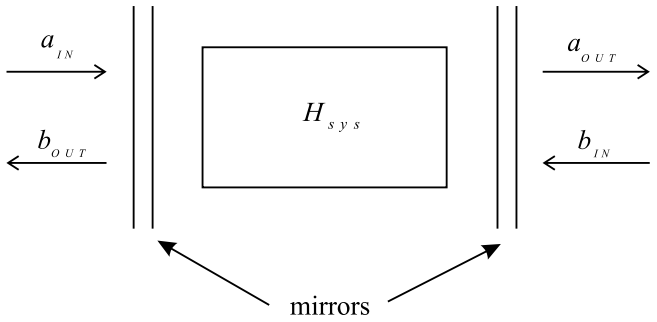

Fig. 11. Scheme of a two-sided optical cavity.

This research was carried along in the framework of the ESPRIT LTR project PIANOS (Processing of Information by Arrays of Nonlinear Optical Solitons). We also acknowledge partial support form the MURST project "Spatial Pattern Control in Sistemi Ottici Nonlineari" and from the CNR finalized project MADESS.

Appendix A

In this Appendix we want to determine the input-output relations relative to a two-sided optical cavity like that considered in this paper.

If we indicate with a the annihilation operator for the internal mode, with $a_{\rm IN}$ and $b_{\rm IN}$ the incoming fields from the two sides, and with $a_{\rm OUT}$ and $b_{\rm OUT}$ the respective outcoming fields (see Fig. 11), the Heisenberg equation describing the time evolution of the operator a becomes [21]

$$\frac{{\rm d}a}{{\rm d}t} = \frac{1}{i\hbar}[a, H_{\rm sys}] - \kappa a + \sqrt{\kappa}(a_{\rm IN} + b_{\rm IN})\,, \qquad \text{(A.1)}$$

where the $H_{\rm sys}$ is the Hamiltonian of the system inside the cavity and κ is the cavity dumping constant (we assumed that the two mirrors have the same dumping constant). The boundary conditions at the mirrors take the form:

$$a_{\rm OUT} = \sqrt{\kappa}a - b_{\rm IN}\,, \qquad \text{(A.2a)}$$

$$b_{\rm OUT} = \sqrt{\kappa}a - a_{\rm IN}\,. \qquad \text{(A.2b)}$$

If we now rescale time to the photon lifetime as in equations (1a, 1b), equations (A.1) can be written as

$$\frac{{\rm d}a}{{\rm d}t} = \frac{1}{i\hbar\kappa}[a, H_{\rm sys}] - a + \bar{a}_{\rm IN}\,, \qquad \text{(A.3)}$$

where we set $b_{\rm IN} = 0$ (in fact in our model we inject the field only from one side) and $\bar{a}_{\rm IN} = a_{\rm IN}/\sqrt{\kappa}$. We note, in

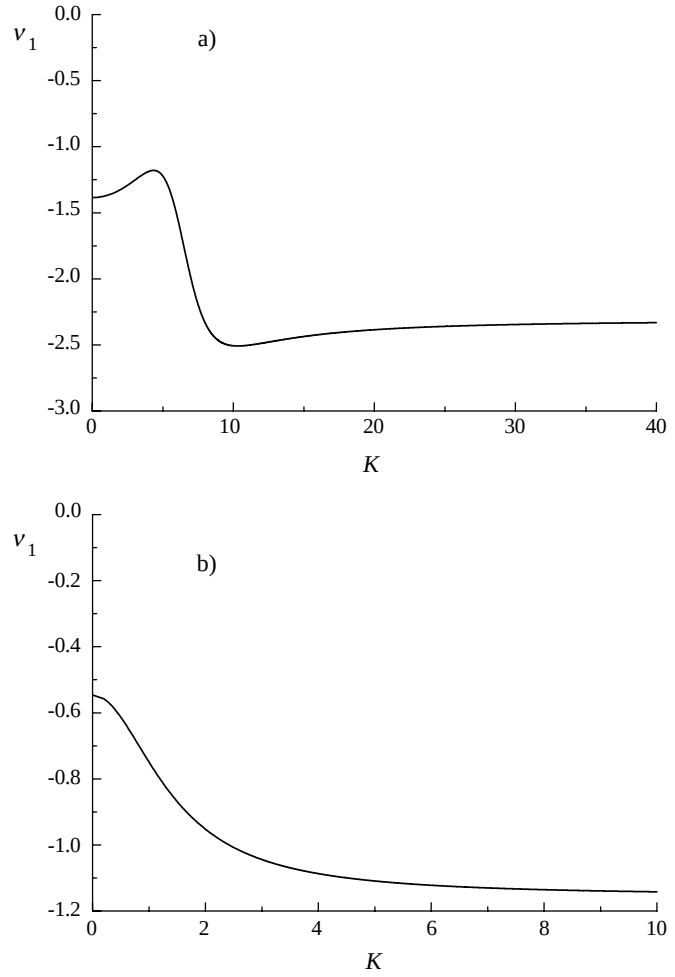

Fig. 12. First-order correction in γ of the real eigenvalue of equation (B.2) as a function of the modulus of the transverse wave vector: (a) passive configuration; (b) active configuration. Parameters are the same as in Figures 2 and 3, respectively.

this way, that the internal field a and the injected field $\bar{a}_{\rm IN}$ have the same normalization than in equations (1a, 1b). By introducing the same normalization also for the output field $a_{\rm OUT}$ and remembering equations (A.2a), we obtain

$$\bar{a}_{\rm OUT} = \frac{1}{\sqrt{\kappa}} a_{\rm OUT} = \frac{1}{\sqrt{\kappa}} \sqrt{\kappa} a = a \,, \tag{A.4}$$

that is the output field normalized in the same way as the input field is equal to the internal field.

Appendix B

In this Appendix we want to study the response of the system to small fluctuations around the homogeneous steady state of equations (1a, 1b). The homogeneous solution $(E_{\rm S}, N_{\rm S})$ is obtained by putting equal to zero the time derivatives and neglecting the Laplacian in equations (1a, 1b). We obtain

$$|E_{\rm I}|^2 = |E_{\rm S}|^2 \left\{ [1+\eta - 2C{\rm Im}(\Theta)(N_S-1)]^2 + [\theta + 2C{\rm Re}(\Theta)(N_{\rm S}-1)]^2 \right\} , \tag{B.1a}$$

$$N_{\rm S} = \frac{-(1+|E_{\rm S}|^2) + \sqrt{(1+|E_{\rm S}|^2)^2 + 4\beta(|E_{\rm S}|^2+J)}}{2\beta} , \tag{B.1b}$$

which, for appropriate choices of parameters, exhibits the characteristic S-shaped form of optical bistability depicted in Figure 1.

The linear stability analysis of the homogeneous solution (B.1a, B.1b) is performed in [12] by studying the response of the system to small fluctuations growing (or decaying) exponentially in time and modulated in space by the transverse wave vector (K_x, K_y). It leads to the following eigenvalue equation:

$$\nu^3 + a_2\nu^2 + a_1\nu + a_0 = 0 \,, \tag{B.2}$$

where the coefficients a_i, $i = 0, 1, 2$ depend on the system parameters and on the modulus square K^2 of the transverse wave vector:

$$a_2 = 2A_1 + \gamma(A_4 + dK^2) \,, \tag{B.3a}$$

$$a_1 = A_1^2 + (A_2+K^2)^2 + \gamma[2A_1(A_4+dK^2) + A_3{\rm Im}(\Theta)] \,, \tag{B.3b}$$

$$a_0 = \gamma\{[A_1^2 + (A_2+K^2)^2](A_4+dK^2) - A_3[(A_2+K^2){\rm Re}(\Theta) - A_1{\rm Im}(\Theta)]\} \,, \tag{B.3c}$$

with

$$A_1 = 1 + \eta - 2C{\rm Im}(\Theta)(N_{\rm S}-1) \,, \tag{B.4a}$$

$$A_2 = \theta + 2C{\rm Re}(\Theta)(N_{\rm S}-1) \,, \tag{B.4b}$$

$$A_3 = 4C|E_{\rm S}|^2(N_{\rm S}-1) \,, \tag{B.4c}$$

$$A_4 = 1 + |E_{\rm S}|^2 + 2\beta N_{\rm S} \,. \tag{B.4d}$$

The homogeneous solution will be stable only if all the eigenvalues ν have a negative real part.

Because both in the active and in the passive configuration the value of the parameter γ is of order 10^{-2} or less, we can estimate the solutions of equation (B.2) by performing an expansion in power series of γ. If we assume $\nu = \nu_0 + \gamma\nu_1$, at zero order in γ equation (B.2) becomes

$$\nu_0^3 + a_2^{(0)}\nu_0^2 + a_1^{(0)}\nu_0 + a_0^{(0)} = 0 \,, \tag{B.5}$$

where $a_i^{(0)}$, $i = 0, 1, 2$ are the coefficients a_i at zero order in γ. Because $a_0^{(0)} = 0$, equation (B.2) has an eigenvalue which is vanishing at zero order in γ. The other two eigenvalues are complex conjugate and, by considering the expressions for the coefficients a_i, $i = 0, 1, 2$, they result at zero order in γ:

$$\nu_0^{\pm} = -A_1 \pm i|A_2 + K^2| \,. \tag{B.6}$$

These eigenvalues cause a fast and oscillating relaxation of the perturbations affecting the homogeneous solution, the oscillation frequency being given by the imaginary part of $\nu_0^{\pm}$.

At first order in γ, equations (B.2) becomes

$$3\nu_0^2\nu_1 + a_2^{(1)}\nu_0^2 + 2a_2^{(0)}\nu_0\nu_1 + a_1^{(1)}\nu_0 + a_1^{(0)}\nu_1 + a_0^{(1)} = 0\,, \tag{B.7}$$

where $a_i^{(1)}$, $i = 0, 1, 2$ are the coefficients a_i at first order in γ. If now we set $\nu_0 = 0$ in equation (B.7), we find the first-order correction of the real eigenvalue which is vanishing at zero order: there results $\nu_1 = -a_0^{(1)}/a_1^{(0)}$. This eigenvalue is responsible for the slow relaxation of the perturbation towards the steady state. Because it is real no oscillations are expected. In Figure 12 we report ν_1 as a function of the modulus of K for both passive and active configurations.

References

1. H.M. Gibbs, *Optical Bistability: Controlling Light with Light*, (Academic Press, New York, 1985); F.A.P. Tooley, S.D. Smith, C.T. Seaton, Appl. Phys. Lett. **43**, 807 (1983).
2. A.C. Walker, M.P.Y. Desmulliez, F.A.P. Tooley *et al.*, in *Proceedings of the 2nd International Conference on Massively Parallel Processing using Optical Interconnections (MPPOI)*, (IEEE Computer Society Press, 1995), pp. 180-187; D. J. Goodwill, A.C. Walker, C.R. Stanley, M.C. Holland, M. McElhinney, Appl. Phys. Lett. **64**, 1192 (1994); W F. Sharfin, M. Dagenais, Appl. Phys. Lett. **46**, 819 (1985); *ibid.* **48**, 321 (1986).
3. L.A. Lugiato, M. Brambilla, A. Gatti, *Optical Pattern Formation*, Adv. At. Mol. Opt. Phys. **40**, (Academic Press, Boston, 1998), p. 229.
4. W.J. Firth, *Self-organization in Optical Systems and Applications in Information Technology*, edited by M.A. Vorontsov, W.B. Miller, (Springer-Verlag, 1995), p. 69.
5. M. Brambilla, L.A. Lugiato, M. Stefani, Europhys. Lett. **34**, 109 (1996); Chaos **6**, 368 (1996).
6. M. Brambilla, L.A. Lugiato, F. Prati, L. Spinelli, W.J. Firth, Phys. Rev. Lett. **79**, 2042 (1997).
7. D.S. Kim, C. Dies, M. Gokhale, S. Forest, IEEE J. Quantum Electron. **33**, 1407 (1997).
8. G. Assanto, Opt. Lett. **20**, 1595 (1995); G. Assanto, Z. Whang, D.J. Hagan, E.W. VanStryland, Appl. Phys. Lett. **67**, 2120 (1995).
9. A.N. Starodumov, Yu. Barmenkov, A. Martinez, I. Torres, L.A. Zenteno, Opt. Lett. **23**, 352 (1998).
10. M. Belic, M. Petrovic, F. Kaiser, Opt. Commun. **123**, 657 (1996).
11. J. Gutierrez, D.Y. Tang, C.O. Weiss, F. Prati, M. Brambilla, Opt. Commun. **135**, 305 (1997).
12. L. Spinelli, G. Tissoni, M. Brambilla, F. Prati, L.A. Lugiato, Phys. Rev. A **58**, 2542 (1998).
13. I. E. Protsenko, L.A. Lugiato, C. Fabre, Phys. Rev. A **50**, 1627 (1994).
14. A. Pregnolato, L. Spinelli, L.A. Lugiato, I.E. Protsenko, J. Mod. Opt. **43**, 269 (1996).
15. V. Pellegrini, F. Fuso, E. Arimondo, F. Castelli, L.A. Lugiato, G.P. Bava, P.L. Debernardi, Phys. Rev. A **50**, 5219 (1994).
16. F. Prati, A. Tesei, L.A. Lugiato, R.J. Horowicz, Chaos Solitons Fractals **4**, 1637 (1994).
17. C.H. Henry, IEEE. J. Quantum Electron. **18**, 259 (1982).
18. W.J. Firth, G. S. McDonald, A.J. Scroggie, L.A. Lugiato, Phys. Rev. A **46**, R3609 (1992).
19. W.J. Firth, A.J. Scroggie, Phys. Rev. Lett. **76**, 1623 (1996).
20. V.B. Taranenko, K. Staliunas, C.O. Weiss, Phys. Rev. A **56**, 1582 (1997).
21. M.J. Collett, C.W. Gardiner, Phys. Rev. A **30**, 1386 (1984).